IOP Conf. Series: Materials Science and Engineering **330** (2018) 012014 doi:10.1088/1757-899X/330/1/012014

A study on chloride induced depassivation of Fe-P-C-Si and Fe-P-C-Si-N steels in simulated concrete pore solution

Yashwant Mehta*, Gajanan P Chaudhari, Vikram V Dabhade

[1]Department of Metallurgical & Materials Engineering, IIT Roorkee, India 247667

* Corresponding author E-mail: yashwant.mehta@gmail.com

Abstract. The corrosion behaviour of high phosphorous steels containing varying amounts of silicon and nitrogen was studied by potentiodynamic polarization, linear polarization resistance (LPR) and electrochemical impedance spectroscopy (EIS) measurements. The morphology of a steel specimen tested in chloride containing concrete pore solution was studied using scanning electron microscope (SEM) and the elemental distribution at the pitting corrosion area was investigated using electron dispersive spectroscopy (EDS). The results showed that the capacitance increased and resistance declined with immersion time in $Ca(OH)_2$ solution containing 0.1% chloride for plain carbon steel. The opposite was observed in the case of the high phosphorous steels. The potentiodynamic polarization and LPR results complement the EIS findings. Corrosion behaviour could be described with an equivalent circuit having two time constants. The creation, expansion and degradation of the passive layer were discussed with the help of the equivalent circuit elements. The SEM-EDS studies revealed that MnS inclusions at the surface could have a role in the initiation and growth of pits and that phosphorous was present at the pit free surface of the steel.

1. Introduction

The corrosion resistance of the Gupta era Delhi Iron Pillar that resisted corrosion for 1600 years is attributed to its phosphorous content [1] [2]. P-rich iron beams used in Puri and Konark withstood marine coastal environments for hundreds of years [3]. However, phosphorous is known to cause cold shortness in cast and wrought steel because of its tendency for grain boundary segregation and therefore its content is restricted to <0.05% [4][5]. Ductile phosphoric irons can be produced by adding a small amount of carbon (0.01 wt % - 0.05 wt %) to the steel [6][7][8][9]. Ductility can be further improved by applying duplex phase heat treatments which remove phosphorous from the grain boundaries improving cohesion [10]. Grabke and Erhart reported that nitrogen can expel phosphorous from the grain boundary sites and decrease the percentage of intergranular fracture [11]. An impact energy value of 118±7.8 J is reported for a Fe-0.15%P steel [12]. Liu and co-workers [13] found that adding 0.5% Si to high phosphorous iron alloys reduced the ductile-brittle transition temperature (small scale Charpy impact test) by approximately 100 K, and the fracture mode became transgranular. The corrosion resistance of Fe-P steels was observed to be better than that of currently used thermo-mechanically treated bars in chloride-containing simulated concrete environments [14].

Concrete contains pores which hold hydrated cement paste. Concrete always contains moisture unless it is dried in an oven [15]. Ions in the paste dissolve in the pore moisture and the resulting solution has a pH of about 12.5. This ensures that the reinforcement bar is in the passive state owing to the creation of a protective passive layer on the surface of the embedded rebar steel [15] [16]. This passivity

may be destroyed in cases of leaching out of fluids from concrete, atmospheric carbonation or uptake of chloride ions [17][18]. Chloride ions induce corrosion of passive reinforcing steel especially when de-icing salts or chloride contaminated aggregate are incorporated into the concrete [17][19]. Marine exposure is also a main source of Cl^- ions.The presence of chloride ions above a threshold value near the rebar surface inside concrete depassivates the steel [20][21][22][23]. Ingress of atmospheric carbon dioxide converts calcium hydroxide to calcium carbonate and reduces pH promoting corrosion[19]. The breakdown of passivity leads to corrosion of the rebars.

Silicon additions to steel favor the formation of goethite with smaller particle size [24]. Nitrogen improves the resistance to localized corrosion like pitting and crevice corrosion in steel [25][26]. The Fe-P-C-Si and Fe-P-C-Si-N steels developed in the present work have impact energy values of about 230 J at room temperature in the heat treated condition and are promising in concrete reinforcement (Table 1 and 3). Therefore it is important to study the corrosion behavior of these steels in $Ca(OH)_2$ solution. Corrosion of steel in concrete can be evaluated by EIS as it is a non-destructive (AC< 20mV), effective in-situ monitoring method and suitable for obtaining the kinetic information related to corrosion reactions occurring on the steel surface [22] [27].

Therefore, in the present work the corrosion behavior of novel Fe-P-C-Si and Fe-P-C-Si-N steels in simulated concrete pore solution with/without various amounts of chloride ions is investigated. Plain carbon steel is included for comparison. The behaviour is studied using EIS. Further, potentiodynamic polarization curves and linear polarization resistance measurements are employed to understand the corrosion behaviour. The mechanism of formation and degradation of the passive film on these novel steels is explained on the basis of the results of the aforesaid methods.

2. Experimental procedure

2.1 Preparing the alloys

Three high phosphorous steels were manufactured using an induction furnace. Desired compositions were produced from melting scrap iron, graphite, ferro-silicon, nitrided manganese, and ferro phosphorous. Aluminium shots were added for de-oxidation. Plain low carbon steel was included in the study for comparison purposes. The chemical composition of the four steels obtained using Magellan optical emission spectrometer is shown in table 1. The mean composition after two readings is presented in the table 1.

Table 1: Chemical composition of the steels.

Sample	P	C	Mn	Si	N	Cr	S	Al	Fe
S1	0.13	0.05	0.2	0.26	0.003	0.13	0.016	0.002	Rest
S2	0.13	0.05	0.2	0.39	0.003	0.14	0.015	0.05	Rest
S3	0.13	0.05	0.46	0.48	0.014	0.2	0.014	0.03	Rest
S4	0.02	0.09	0.32	0.07	0.002	0.03	0.017	0.004	Rest

2.2 Dilatometry and thermo-mechanical processing

Dilatometry studies were conducted using a thermo-mechanical simulator (GLEEBLE 3800® of Dynamic Systems Inc.). The castings were sliced to obtain smaller pieces of about 3 cm x 4 cm x 5 cm. These were hot forged at about 1150°C to obtain rods having diameter of 10 mm and square rods with a side of 12 mm. The rods were subsequently heat treated at 900°C for one hour. The heat treated samples were subsequently air cooled. It was expected that the heat treatment in the duplex phase ($\alpha + \gamma$) region would cause site competition between phosphorous and carbon/nitrogen leading to a reduction in grain boundary segregation of phosphorous causing improvement in ductility. This heat treatment temperature of 900°C was selected after dilatometry studies. Heat treated rods were utilized to prepare tensile and impact test samples. Cylindrical tensile samples having a gauge diameter of 5 mm and Charpy V notch impact specimens having size 10 mm x 10 mm x 55 mm were prepared according to ASTM A-370. The tensile samples were tested at 6.6×10^{-4} s^{-1}; using a Hounsfield tensile testing machine (25kN). The impact specimens were tested using a Veb Werkstoffprufmaschinen machine at room temperature.

2.3 Corrosion behaviour

The corrosion study sample (15 mm x 15 mm x 8 mm) surfaces were polished with emery paper (up to 800 grit) and cleaned with acetone. Three samples were prepared for ensuring reproducibility in experimentation. A standard flat cell (Ametek USA) was used for testing the samples. Potentiodynamic polarization, linear polarization resistance and electrochemical impedance spectroscopy studies were conducted. Potentiodynamic polarization experiments were run using an EG&G PARSTAT 273A Potentiostat (Ametek, USA) at a scan rate of 0.75 mVs^{-1} with SCE reference electrode. Saturated $Ca(OH)_2$ solutions with 0, 0.05, 0.1, 0.14 weight % Cl^- Content were employed (All future references to % Cl^- in this text should be construed to be weight %). Earlier work has shown that results of electro-chemical tests conducted in saturated $Ca(OH)_2$ are similar to those obtained in concrete [28]. The pH of the solution (12.5) was measured using pH 510 of Eutech instruments. Before commencing the potentiodynamic polarization experiments, the open-circuit potential (OCP) was allowed to stabilize for 1h.

The EIS and LPR experiments were conducted using Gamry 1000 Interface at intervals of 15 minutes, 5h and 21h. For LPR, the potential was scanned at 0.125 mV $s^{-1}$from −20mV to +20 mV with respect to the OCP. The slope of the E vs *i* curve at zero current yielded the polarization resistance (R_p). LPR technique was chosen to monitor the corrosion rate during immersion of samples for 21 h since the surface of the sample does not deteriorate. LPR was useful in studying the change in the corrosion resistance of the passive surface with time in the test solution without and with chloride. The measured LPR can be used to calculate the instantaneous corrosion rate using the Stern-Geary equation [29][30] as shown below:

$$i_{corr} = \frac{1}{2.303} \times \frac{\beta_a \beta_c}{R_p \times (\beta_a + \beta_c)} = \frac{Z}{R_p} \quad (1)$$

Z depends upon the anodic ($\beta_{a,}$) and cathodic (β_c) Tafel slopes. For each solution composition, the test was repeated twice. For the EIS tests, a sinusoidal potential perturbation of 10 mV was applied at the OCPs with frequency sweep from 100 KHz to 10 mHz using the GAMRY Interface 1000 potentiostat. GAMRY EChem analyst software was used to analyse the EIS data by fitting with equivalent circuits. These analyses determined the passive layer parameters. The high frequency arc was fully revealed by scanning from 2MHz to 1000 Hz using PARSTAT 2273. The solution resistance and the adsorbed layer data was calculated using this data.

The surface morphology of S3 steel specimen used for potentiodynamic polarization in the $Ca(OH)_2$ solution containing 0.14% chloride was observed by SEM (Zeiss EVO 18) in order to examine its state of corrosion. Elemental distribution at pitted area was studied using EDS.

3. Results and Discussion

3.1 Dilatometry and mechanical behaviour

The results of the dilatometry studies are shown in table 2. These were used to select the temperature of 900°C for the duplex phase heat treatment of the tensile and impact test samples. The mechanical properties of these steels hot forged and subsequently heat treated for 1 hour at 900°C condition are shown in table 3. The strength of all the high phosphorous steels is around 400 MPa and the elongation exceeds 33%. The yield stress, ultimate tensile stress, % elongation and % reduction in area of S1, S2 and S3 steels compare well with the findings of other researchers for Fe-0.11P-0.03C steel [10]. The toughness of S1, S2 and S3 steels is better than the energy value of 118±7.8 J recorded for Fe-0.09C-0.37Si-0.42Mn-0.15P- 0.37Cr- 0.35Cu- 0.31Ni-0.03Al steel [12]. The impact values of the high phosphorous steels studied in the present work are comparable with those of the plain carbon steel. Encouraged by these good mechanical properties, the corrosion behaviour of the high phosphorous steels is studied and discussed in the following sections.

Table 2: Transformation temperatures of the three high phosphorous steels determined by dilatometry studies conducted in Gleeble 3800® thermo-mechanical simulator.

Transformation Temperature	S1	S2	S3
A_{r1} (°C)	790	813	805
A_{r3} (°C)	965	941	925

Table 3: Mechanical properties of the steels, hot forged and subsequently heat treated at 900°C for 1 hour.

Specimen	YS (MPa)	UTS (MPa)	Elongation (%)	Reduction in Area (%)	Impact energy (J)
S1	229.8±8.3	392.5±10.6	35.3±2.6	62.5±1.7	183.7±19.5
S2	327.5±26.7	430.2±18.8	34.6±0.8	68.2±4.1	232.5±22.9
S3	258.6±19.2	396.6±13.8	33.6±1.5	60.7±2.9	226.5±17.2
S4	407.1±1.3	478.7±2.3	19.4 ±2.0	63.2±3.6	222.2±2.7

3.2. Anodic polarization behavior

Figure 1 shows the anodic polarization curves of the processed steel samples tested in saturated $Ca(OH)_2$ solution containing various Cl^- ion concentrations. All the samples exhibit passive behaviour in this solution. This conforms to the Fe-water E_h-pH diagram of 298.15 K. The range of passivity decreases as the Cl^- content increases beyond a threshold value. In all the curves for all the samples immersed in solution with 0.05% Cl^- and without chloride, current density increases at about 650 mV_{SCE} which is attributable to O_2 evolution and is dependent on pH. Beyond a critical chloride concentration, the corrosion current registered a drastic increase during the experiment preceding the oxygen evolution. In the presence of Cl^- ions, the pitting potential became more negative towards the active side. For each steel composition, the pitting or passive film breakdown occurred when the chloride concentration exceeded a critical amount. The threshold value of Cl^- ion concentration for the initiation of pitting is determined as 0.1% Cl^- for S1, S2 and S3 steels while it was 0.06% Cl^- for the S4 steel. At these concentrations the pitting potential of the steel samples was lower than the oxygen evolution potential. Tests were also carried out in solutions containing 0.14 Cl^- in order to confirm the lower pitting potential of the steels. Other researchers have reported threshold values of 0.05% Cl^- for AISI 1010 steel [31], 0.06% Cl^- for Fe-0.15C steel and 0.1% Cl^- for Fe-0.11P steel [14]. Thus, S1, S2 and S3 steels are more resistant to pitting than S4 steel as their threshold chloride is found to be higher in this work.

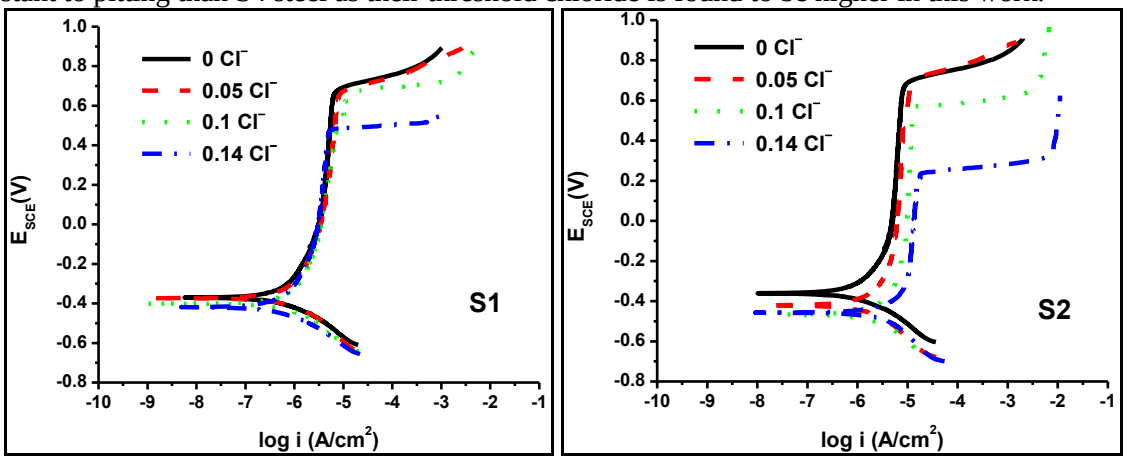

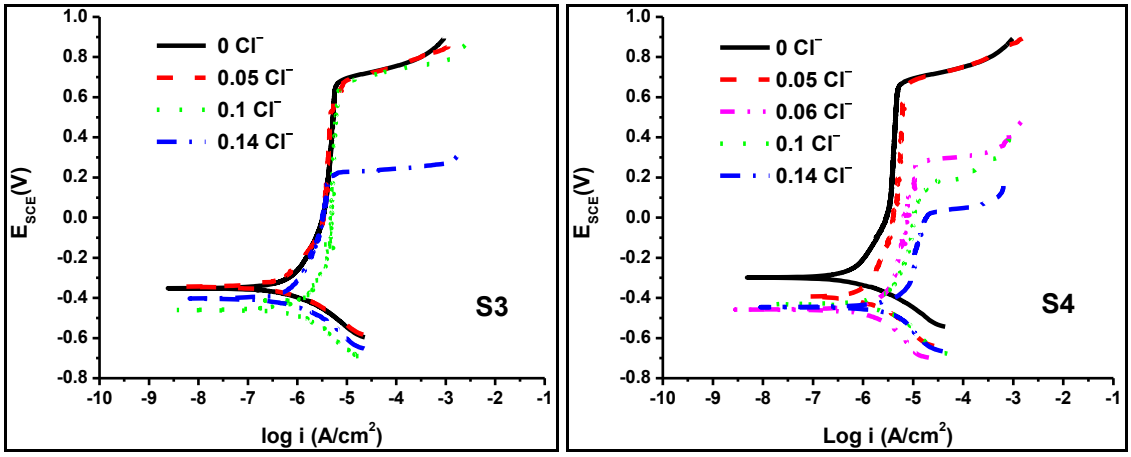

Figure 1. Potentiodynamic polarization curves of S2, S2, S3 and S4 steels obtained in simulated concrete pore solution having various chloride concentrations.

3.3 OCP and LPR studies

For all steel samples, the open circuit potential and the linear polarization resistance were recorded after 15 minutes, 5 h and 21 h. The LPR values were used to calculate i_{corr} using equation (1). Figure 2 shows the variation of the OCP and i_{corr} for the samples S3 and S4 steels exposed to aerated saturated solution of $Ca(OH)_2$ containing various chloride concentrations. The OCP of S3 steel shifted towards noble direction while the i_{corr} values decreased with time of dipping in all solutions. Similar trends were observed in the case of S1 and S2 steels too. This trend implies that with increasing immersion time the steel became nobler [32]. It has been reported that as the anodic curve shifts to lesser current densities, the E_{corr} increases and i_{corr} decreases [33]. In the case of S4 steel immersed in solutions containing 0.05% and 0.1 % Cl^-, there is an overall decline in OCP with the immersion time which suggests increased corrosion. The i_{corr} values of S4 steel did not show a corresponding overall increase. The OCP values indicate that the critical chloride concentration for initiation of pitting could be 0.05% and is probably lower than that of the high phosphorous steel samples.

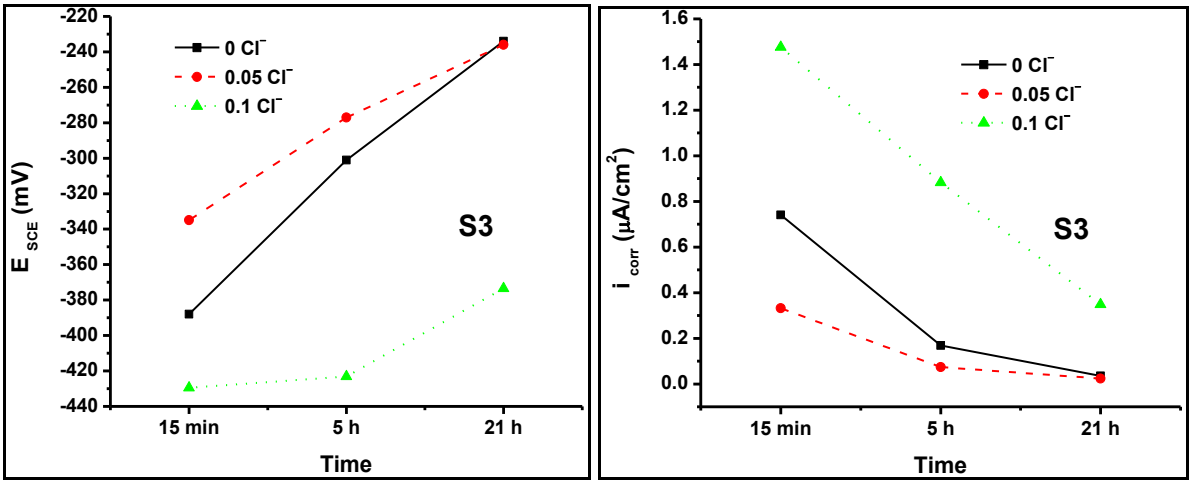

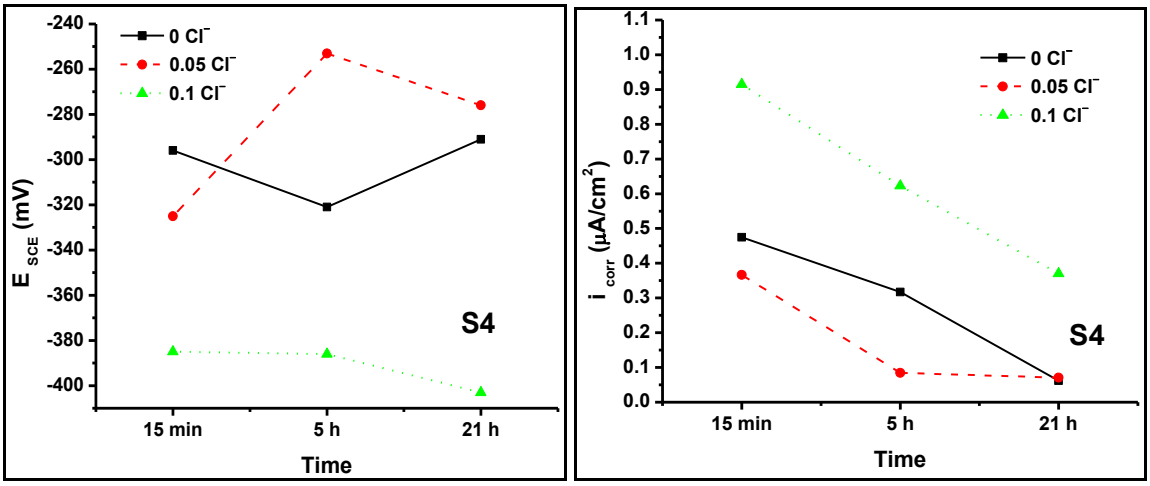

Figure 2. Variation of the OCP and i_{corr} for the S3 and S4 steel samples exposed to simulated concrete pore solution containing various chloride concentrations.

3.4 Electrochemical impedance spectroscopy

Figure 3 shows the Nyquist, Bode magnitude and Bode phase plots of S3 and S4 steels in saturated solution of $Ca(OH)_2$ containing 0.1% Cl^- at different times of immersion. The impedance responses of S3 steel in saturated solution of $Ca(OH)_2$ without chloride and that having 0.05% Cl^- were similar to those obtained in solution having 0.1% Cl^-. For S1, S2 and S3 steels, the impedance escalated with time in all solutions. This variation in response was also found similar to that of S4 steel in $Ca(OH)_2$ solution containing zero and 0.05% chloride. A different impedance response was recorded for S4 steel in $Ca(OH)_2$ solution with 0.1% chloride concentration.

A capacitive loop of depressed semicircles is seen in the Nyquist plots of S3 steel. Further, with increase in immersion time the capacitive part increases. Again, with escalation in immersion time, the polarization resistance or the real impedance increases. Opposite trend is seen in the Nyquist plots of S4 steel i.e. as the time of immersion increases there is a decline in the polarization resistance and capacitive component. Upon dipping a metal in a solution, the metal ions enter the solution and in time an electrical double layer is formed at the metal-solution interface. The current at the metal electrolyte interface can be modelled as a capacitance as $C=q/V$. Here, q represents the charge in the double layer upon dissolution of the metal. V is the potential at which the sample corrodes freely. If the passive film grows becomes more protective with time then the micro-pores present on the film will grow smaller with time and metal dissolution will decrease. This implies that the capacitance associated with the double layer will decrease since $C=1/2\pi fZ$ where f is the frequency. The capacitive part increased and capacitance decreased with time of immersion for S1, S2 and S3 steels. Again

$$C = \frac{\varepsilon\varepsilon_0}{d} \tag{2}$$

where d is the thickness of the film, , ε_0 is the vaccum permittivity and ε is the dielectric constant of the film [34]. Therefore, a thicker and more protective passive layer with time of immersion implies a decrease in capacitance C as observed in the case of S1, S2 and S3 steels. The capacitance increased and capacitive part decreased with immersion time, due to an increased q owing to corrosion of S4 steel in ($Ca(OH)_2$ + 0.1 Cl^-) solution. Real impedance decreased with immersion time indicating breakdown of passive film.

For S3 steel tested in the saturated solution of $Ca(OH)_2$ without Cl^- and with 0.05 % Cl^- and 0.1% Cl^-, at frequencies less than about 10^2 Hz the Bode magnitude plots exhibited a purely capacitive behaviour. With increasing immersion time, the straight-line portion with a slope of about −1 (the capacitive part) expanded. This response was found similar to the responses of S1 and S2 steels. Similar response was observed for S4 steel in $Ca(OH)_2$ solution and ($Ca(OH)_2$ + 0.05% Cl^-) solution, too. At

the end of 21 h of immersion, the impedance of passive film ranged from 10^4 Ω.cm^2 to 10^5 Ω.cm^2 for all the samples. The passive film acts as a capacitor effectively when the impedance is greater than 10^6 Ω.cm^2 [33]. The high values of impedance imply that the passive film becomes more protective with time of immersion. For S4 steel in ($Ca(OH)_2$ + 0.1 Cl^-) solution, the central portion of bode magnitude curve declined with time of immersion, which indicates that the passive film broke down.

By measuring the high and low break point frequencies of the Bode magnitude plots, capacitance can be calculated. These frequencies are found where the two frequency independent horizontal parts intersect with the central straight line portion having negative slope [35]. The low and high frequencies can be located at the 45° phase angle too. The capacitance corresponding to high (f_h) and low (f_l) frequencies can be calculated as follows:

$$C_h = \frac{1}{2\pi f_h R_u} \tag{3}$$

$$C_l = \frac{1}{2\pi f_l (R_u + R_p)} \tag{4}$$

Where R_u is the solution resistance and R_p is the polarization resistance. C_l declined with time indicating enlargement of passive layer for S1, S2 and S3 steels in all the solutions and S4 steel in solutions containing less than 0.1 Cl^-. The f_l of S4 steel for the ($Ca(OH)_2$ + 0.1 Cl^-) solution increased with immersion time depicting the breakdown of passive layer and dissolution of iron. Capacitance is considered to be a good pointer for the initiation of pitting [33] [36].

In the Bode phase plots, the phase angle (θ) in S1, S2 and S3 steels in all solutions and S4 steel in solutions containing less than 0.1 Cl^- declined to zero at f_h and f_l. The value of θ at zero correlates with the resistances of R_u and (R_u+R_c+R_p). Capacitive behavior is indicated by the increase of θ towards 90° at intermediate range of frequencies [35]. The crest of Bode phase plots in S1, S2 and S3 steels in all solutions and S4 steel in solutions containing less than 0.1 Cl^- widened with time of immersion. This considerable phase shift at absolute value of θ (crest of the plot) in the Bode phase angle graph implies broadening of passive layer with immersion time. The frequency, at which the decline in absolute value of θ starts, decreased as the immersion time increased. As the immersion time increased, the lower frequency break point corresponding to 45° drifted towards lower frequencies. Therefore, the phase angle drift at low frequencies increased with immersion time for Bode phase plots in S1, S2 and S3 steels in all solutions and S4 steel in solutions containing less than 0.1 Cl^-. This indicates improvement of protective capabilities of the passive layer with immersion time [33][36][14]. The degradation of organic coatings are indicated by a decrease in phase angle shift at low frequency regions [14][36]. The phase angle drift at low frequencies decreased with immersion time for Bode phase plots in S4 steel in solutions having 0.1 Cl^- indicating degradation of passive layer and increasing corrosion with immersion time.

From the above observations on the Nyquist and Bode plots one can say that the decreasing capacitance and increasing impedance was found in the cases S1, S2 and S3 steels in all solutions and in case of S4 steel in solutions containing less than 0.1 Cl^-. This may be due to decrease in the micro-pores and increased protective coverage of the surface by the passive oxide layer with immersion time. The film deteriorated in the case of S4 steel in solutions having 0.1 Cl^- and corrosion increased with time. Thus it can be said that for S1, S2 and S3 steels, the threshold Cl^- concentration for degradation of oxide layer is higher than 0.1%. It is less than 0.05% for S4 steel.

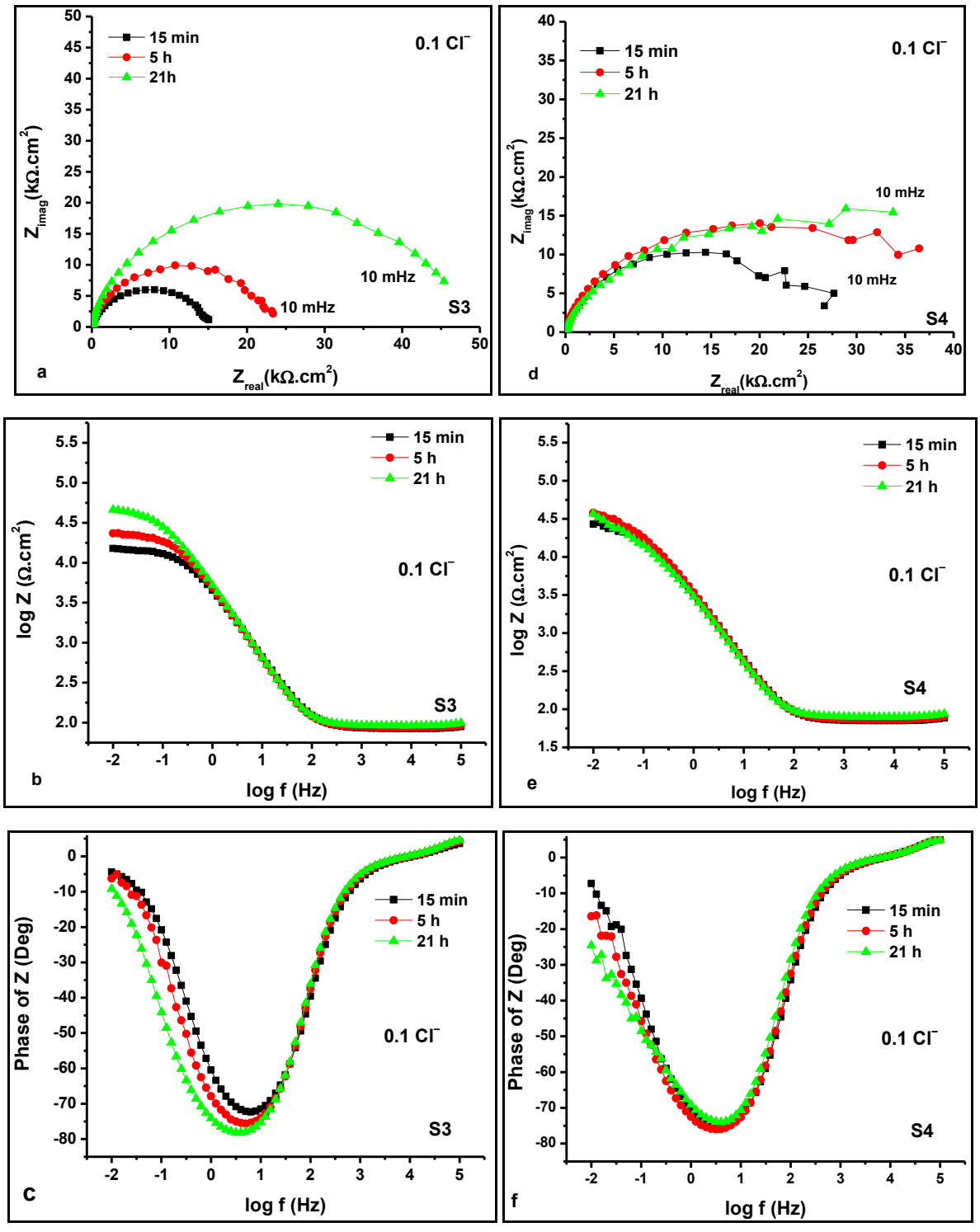

Figure 3. Nyquist, Bode magnitude and Bode phase plots of samples S3 (a, b & c) and S4 (d, e & f) steels respectively, exposed to simulated concrete pore solution containing 0.1% Cl^-.

The EIS spectra of all samples exhibited two time constants. The Nyquist plot of S3 steel immersed for 5 hours in $Ca(OH)_2$ solution with 0.1% Cl^- chloride shows the high frequency region as an inset in figure 4. According to Saremi and Mahallati, the arc in the high frequency region could be associated with the OH^- ion adsorption on the surface of the steel [17].

At frequencies lower than 790 Hz, the arc which appears is related to the interfacial reaction. This reaction is composed of two processes viz. the charge transfer reaction and the formation of a passive film, which have an identical time constant as per the opinion of other researchers [17][37]. In order to fit the experimental data, many equivalent circuits were tried using Gamry Echem Analyst software version 6.04. The best fitting equivalent circuit that approximates the test system is shown in figure 5. It can also be written as $R_u(C_c(R_c(Y_0R_p)))$. Here, solution resistance is represented by R_u. The resistance and capacitance of the adsorbed layer are given by R_c and C_c. R_p and Y_0 are the resistance and capacitance associated with the corrosion processes occurring in the micro-pores of the oxide film. The oxide film resistance is composed of the resistance due to the film and charge transfer. Mathematically, the impedance of the circuit can be written as

$$Z = R_u + \frac{A}{Aj\omega C_c + 1} \tag{5}$$

where ω is the angular frequency and

$$A = R_c + \frac{R_p}{(j\omega)^{\alpha} Y0.R_p + 1} \tag{6}$$

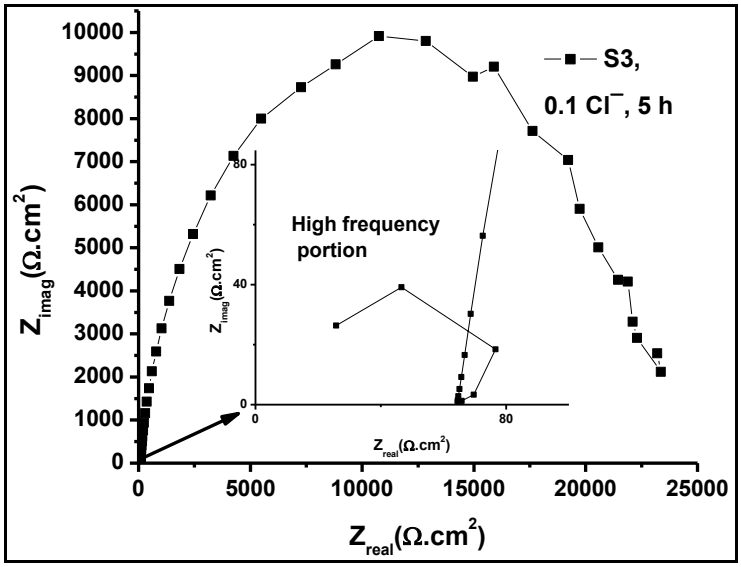

Figure 4. Nyquist plot showing the second time constant in the high frequency region for S3 steel immersed in simulated concrete pore solution containing 0.1% Cl^- for 5 h.

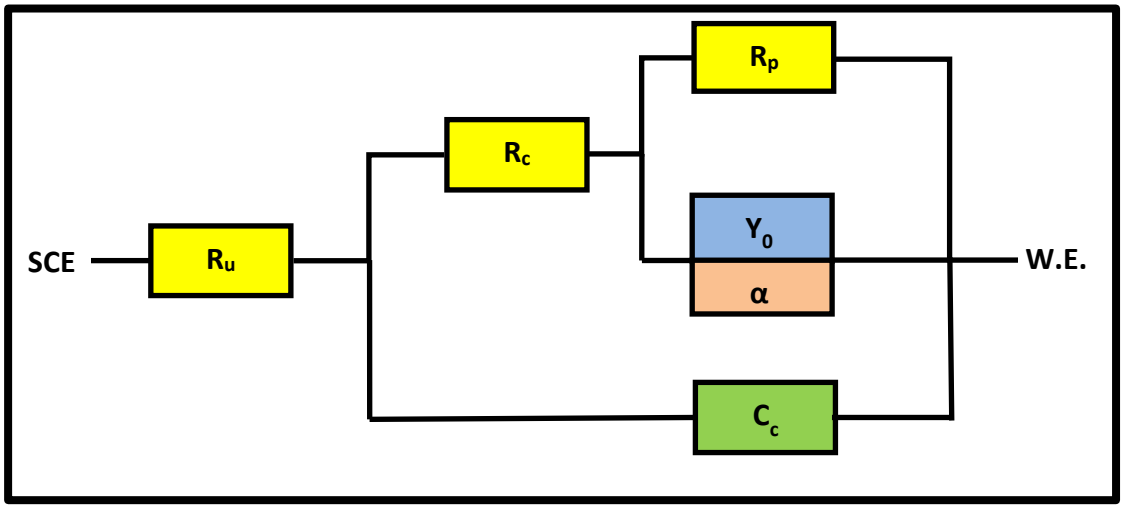

Figure 5. Equivalent circuit for rebar steel designed in this work.

Very little variation was found in the parameters R_u, R_c and C_c with respect to immersion time and chloride content. In the simulated concrete pore solution either with or without chloride, mean R_u was about 17 Ω.cm^2, mean R_c was about 80 Ω.cm^2 and mean C_c was about 0.019 μF/cm^2 for all the samples (Figure 4). R_u, R_c and C_c for mild steel and Fe-P alloys in $Ca(OH)_2$ solution with/without Cl^- found by Sahoo and Balasubramaniam were approximately 25 Ω.cm^2, 35 Ω.cm^2 and 11 μF/cm^2 respectively [14]. R_s, R_c and mean C_c for mild steel in simulated concrete pore solution with/without Cl^- were found by Saremi and Mahallati to be 62 Ω.cm^2 , 31 Ω.cm^2 and 0.02 μF/cm^2 respectively [17]. Saremi and co-workers attributed the adsorbed layer to OH^- ion on the surface of iron. The miniscule resistance of this adsorbed layer does not help in making the steel corrosion resistant.

The variables concerned with the passive film polarization resistance viz. R_p, CPE exponent α and constant phase element Y_0 showed variation. The double layer-capacitance impedance can be expressed by a constant phase element (CPE) rather than an ideal capacitor in case the surface is rough and heterogeneous [14][22][38][39][40]. The impedance (Z_{CPE}) and capacitance (C_{CPE}) are defined by equations (7) and (8) [14][22][41].

$$Z_{CPE} = [Y_0 (j\omega)^{\alpha}]^{-1} \tag{7}$$

$$C_{CPE} = \frac{Y_0 \omega_m^{\alpha-1}}{\sin(\alpha\pi/2)} \tag{8}$$

Y_0 represents a combination of properties related to electroactive species and the steel surface. It is proportional to the capacitance of pure capacitive electrodes [14][22]. α is the CPE exponent. It is a phenomenological coefficient which indicates the degree of deviation in the capacitance from the ideal condition [22][42][43]. The frequency corresponding to maximum phase angle is ω_m [22]. Y_0 is called CPE when α lies between 0.5 and 1 and is based on surface heterogeneity and roughness [14]. Y_0 is pure capacitance when α =1 and pure resistance when α =0 [44].

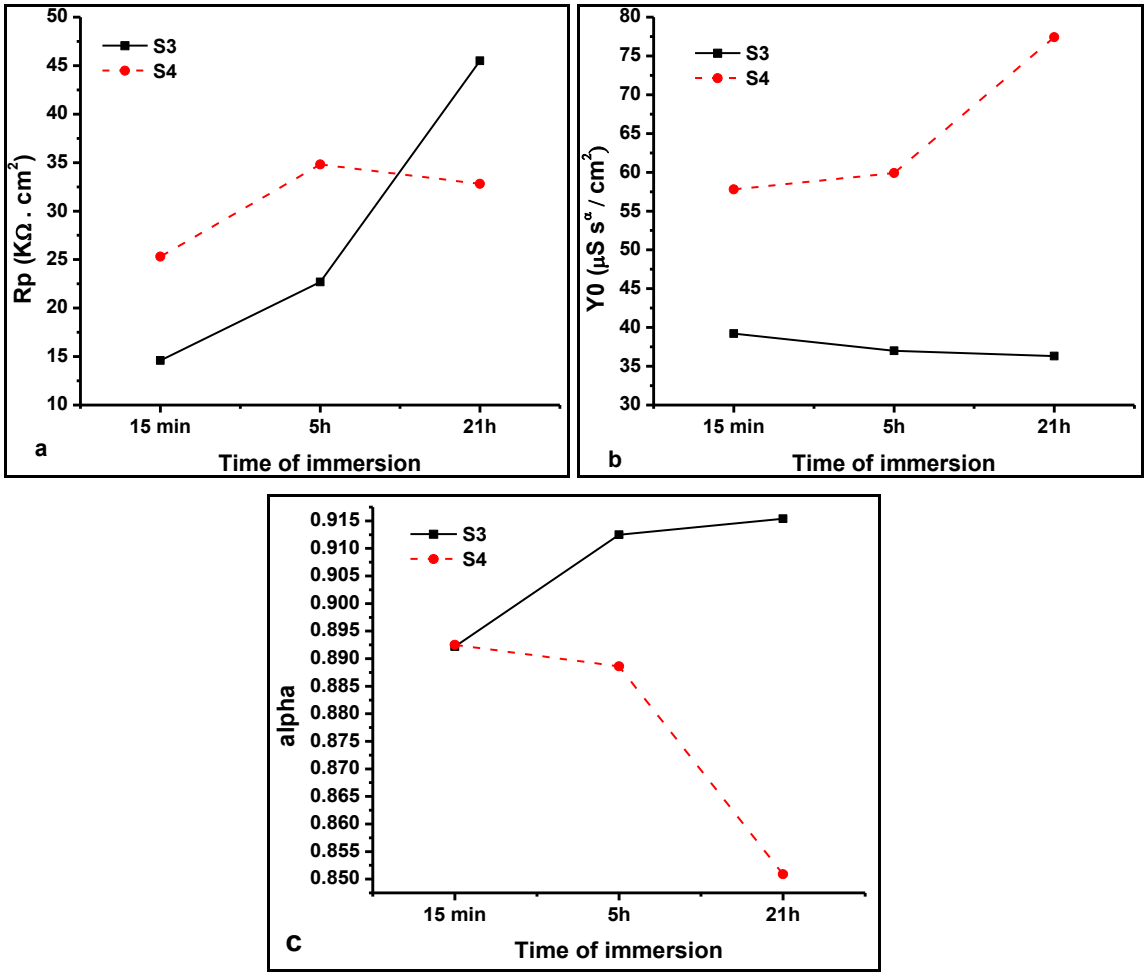

Figure 6. The variation of (a) R_p, (b) Y_0, and (c) α of the passive film with respect to time of immersion of S3 and S4 steels in simulated concrete pore solution containing 0.1% Cl^-.

R_p values generally escalated with immersion time for S1, S2 and S3 steels in all solutions and S4 steel in solutions containing less than 0.1 Cl^-. R_p values decreased with time for S4 steel in solutions containing 0.1 Cl^- (Figure 6a). R_p values of all the samples vary between $1.4x10^4$ to $7.7x10^5$ Ω.cm^2. The R_p values obtained by Sahoo and Balasubramaniam after 7 days immersion of Fe-P alloys and mild steel in $Ca(OH)_2$ solution with/without Cl^- varied between $1.5x10^4$ and $7.3x10^5$ [14]. The R_p values for plain carbon steel in $Ca(OH)_2$ solution without and with 0.3 Cl^- were found by Saremi and Mahallati to be between $1.5x10^5$ to $1.7x10^5$ Ω.cm^2 [17]. Reported values for passive layer of steel in borate buffer alkaline solution are 10^4 to 10^6 Ω.cm^2 [45][46].

Y_0 values were between 36 to 77 μS s$^\alpha$/cm^2 which agrees with the values of 14-75 μS s$^\alpha$/cm^2 for phosphoric irons and mild steel found by Sahoo and co-workers [14]. An overall decrease in Y_0 was observed with immersion time due to the expansion of passive layer except in the case of S4 steel in $Ca(OH)_2$ solution containing 0.1% chloride (Figure 6b). This is caused due to breakdown of passive film and consequent increase in capacitance [14][17]. α values varied between 0.78 to 0.92 which confirms the heterogeneity of the steel surface as observed by other researchers too [38] [39]. The increase in α of S3 steel indicates improvement in passive film and the decrease in α of S4 steel implies that the film became increasingly inhomogeneous and defective with time (Figure 6c) [22].

Figure 7 shows a schematic diagram of the growth or destruction of the passive layer with time. On immersion in the solution the passive film starts forming and iron ions enter the solution after passing

through the micro-pores of the film. Initially the pores are large (Figure 7a) and later with the growth of the film (Figure 7b) they become smaller reducing the exposed area and hence the corrosion current. This increase in thickness of double layer causes an increase in R_p and decrease in capacitance (follows decrease in charge per unit area). In the case of S4 steel immersed in simulated concrete pore solution containing 0.1% Cl^-, the chloride ions destabilize the passive film by migrating through the micro-pores and probably causing the following reaction on the metal surface exposed inside the pores [14].

$$Fe^{2+} + 2H_2O + 2Cl^- \rightarrow Fe(OH)_2 + 2HCl \quad (9)$$

The Cl^- formed may be used in auto-catalysis of the pitting process, thereby increasing the size of the micro-pores and leading to degradation of passive layer and accelerating the corrosion processes (Figure 7d).

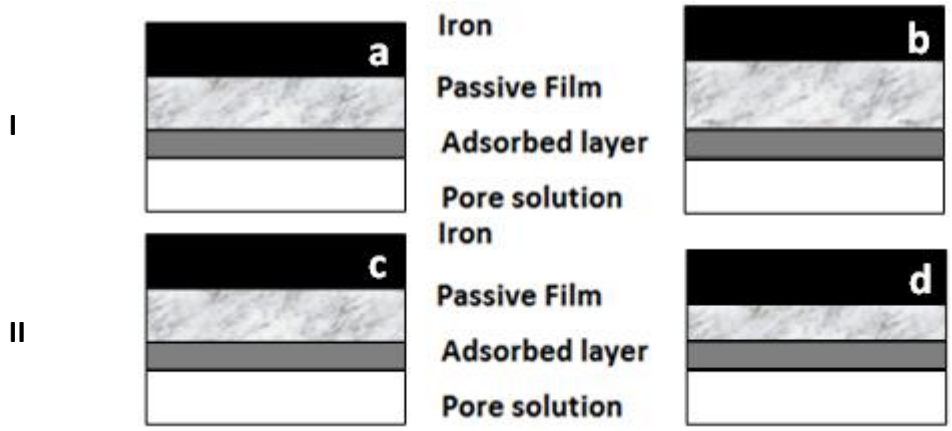

Figure 7: Schematic displaying the formation, growth and degradation of the passive film on the steel surface in simulated concrete pore solution. In first condition the solution is without Cl^- or with Cl^- present in amounts lower than the threshold amount; (a) start of immersion; (b) passive layer grows with time. In second condition the solution contains Cl^- ions more than the threshold amount; (c) same as (a); (d) de-passivated steel.

3.5. Corrosion surface analysis

Surface morphology of S3 steel after potentiodynamic polarization testing in ($Ca(OH)_2$ + 0.14% Cl^-) solution was observed by SEM to examine its state of corrosion. Surface shows a few pits and sporadic deposits. The observations agree with the outcome of the electrochemical studies. EDS was employed to understand the mechanism of corrosion of S3 steel from chlorides by recording the elemental distribution at the pitted location (Figure 8). EDS reveals that Mn, S, Cl, O and Si are present in the pit region. This suggests that adsorption of chloride ions followed by the initiation of pits could have been favoured by presence of MnS inclusions. Literature suggests that chloride is adsorbed preferentially at the MnS inclusions associated with oxides of aluminium causing their dissolution accompanied with a local drop in pH leading to local autocatalysis [47]. Once a pit nucleates it might grow depending on whether the local chloride concentration exceeds critical limits [22]. Further, P, Cr and N are found well-distributed and deficient in the pit region. It can be stated that P could play a positive role in protecting the surface from pitting damage.

S3	**Mn**	**S**	**O**
	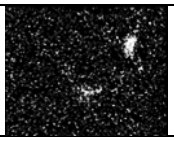	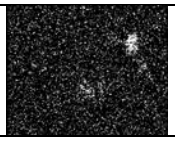	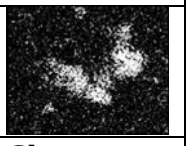
	Na	**Fe**	**Cl**

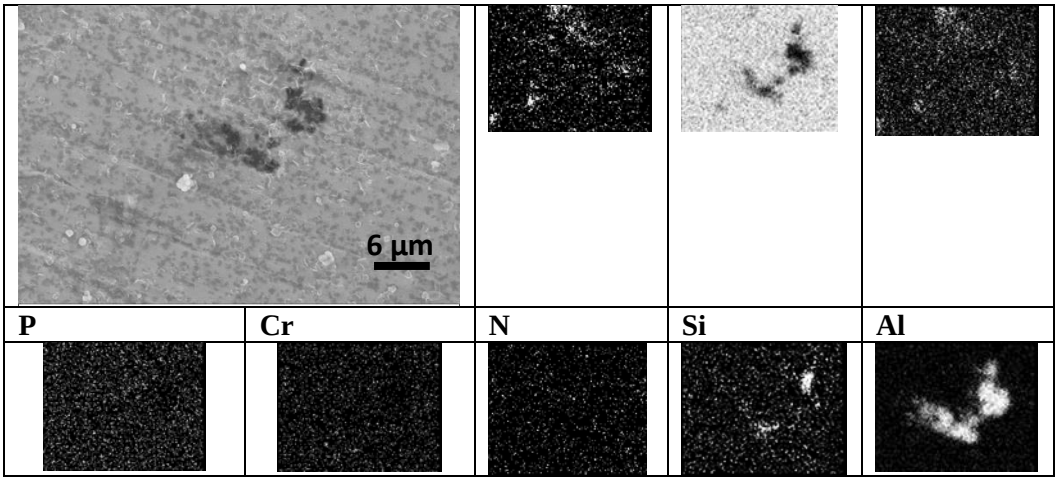

Figure 8. The SEM-EDS study of surface morphology of S3 steel after potentiodynamic polarization testing in ($Ca(OH)_2$ + 0.14% Cl^-) solution, and elemental distribution at corroded area.

3.6 Beneficial effect of phosphorous alloying

The OCP measured vs SCE for all the samples are above −0.5 V. Therefore, according to the Eh-pH diagram of phosphorous-water system, phosphorous in the S1, S2 and S3 steels will remain in equilibrium with PO_4^{3-} in saturated $Ca(OH)_2$ solution having pH 12.5, at and above −0.258 V vs SHE [48].

Anodic corrosion inhibitors employed for iron in concrete environments involve phosphates like $CaHPO_4$, Na_3PO_4 and Na_2HPO_4 [28][49]. The phosphate ions help in the oxidation of ferrous to ferric form. The drift of the ferrous ions away from the metal surface is prevented [50]. The accumulated ferric ions form a protective γ-Fe_2O_3 film in $Ca(OH)_2$ solution [28]. The film causes a reduction in the intensity of corrosion by reducing active sites. Phosphorous containing steels form a bipolar passive film. The inner iron oxide layer is anion selective while the outer $Fe_3(PO_4)_2$ enriched layer is cation selective and hence blocks the entry of Cl^- ions into the film improving resistance against nucleation and growth of pits [51][52].The inner layer probably converts to gamma Fe_2O_3 leading to the thickening of the passive layer [14]. This also explains the absence of P in the pit region and presence of P outside the pit region on the surface of the steel in figure 8.

4. Conclusions

The high phosphorous steels developed in this work showed mechanical properties comparable to rebar steel. Their polarization studies in simulated concrete pore solution containing up to 0.1% chloride concentration revealed a stable passive behaviour and good pitting corrosion resistance. Whereas, plain carbon steel could withstand, only up to 0.06% chloride. LPR and OCP measurements also confirmed the improved performance of phosphorous steel over the plain carbon steel.

High capacitance from the equivalent circuit obtained from the EIS spectra indicated rough surface due to pitting corrosion. Decreased resistance of passive film implies that chloride above the threshold concentration degraded the passive layer of steel. With the thickening of the passive layer, phase angle plots widened. Unlike phosphorous steels, the plain carbon steel corroded actively in 0.1% chloride-containing simulated concrete pore solution.

Corroded surface of S3 steel tested in simulated concrete pore solution with 0.14% chloride solution suggest that MnS inclusions could be crucial in the initiation of pits since they attract chloride ions. The presence of phosphorous outside the pits could indicate that phosphorous blocks the entry of chloride ions and thus prevents corrosion. Thus, the high phosphorous steels developed in this work have potential to deliver improved corrosion performance in concrete environments provided weldability concerns are suitably addressed.

Acknowledgements: Authors acknowledge *M/S Vaishnav Steel Private Limited*, Muzaffarnagar, Uttar Pradesh, India for providing the steel castings for research.

5. References

[1] R. Balasubramaniam, "On the corrosion resistance of the Delhi iron pillar," *Corros. Sci.*, vol. 42, no. 12, pp. 2013–2129, 2000.
[2] R. Balasubramaniam and A. V. R. Kumar, "Characterization of Delhi iron pillar rust by X-ray diffraction , Fourier transform infrared spectroscopy and Mossbauer spectroscopy," *Corros. Sci.*, vol. 42, pp. 2085–2101, 2000.
[3] R. Balasubramaniam, *Delhi iron pillar—New insights*. Shimla: Indian Institute of Advanced Study, 2002.
[4] W. Rostoker and B. Bronson, *Pre industrial iron-its technology and ethnology, Archaeomaterials Monograph No.1*. Philadelphia, PA: University of Pennsylvania, 1990.
[5] M. Goodway and R. M. Fisher, "Phosphorus in low carbon iron: Its beneficial properties," *Hist. Metall.*, vol. 22, pp. 21–23, 1988.
[6] B. E. Hopkins and H. R. Tipler, "The effect of phosphorus on the tensile and notch impact properties of high purity iron and iron carbon alloys," *J Iron Steel Inst.*, vol. 188, pp. 218–237, 1958.
[7] J. W. Stewart, J. A. Charles, and E. R. Wallach, "Iron – phosphorus – carbon system Part 1 – Mechanical properties of low carbon iron – phosphorus alloys," *Mater. Sci. Technol.*, vol. 16, pp. 275–282, 2000.
[8] S. Suzuki, M. Obata, K. Abiko, and H. Kimura, "Role of carbon in preventing alloys the intergranular fracture in iron-phosphorus," *Trans. Iron Steel Inst. Japan*, vol. 25, no. 1, pp. 62–68, 1985.
[9] S. Suzuki, M. Obata, K. Abiko, and H. Kimura, "Effect of carbon on the GB segregation of Phosphorus in alpha-Iron," vol. 17, no. c, pp. 1325–1328, 1983.
[10] G. Sahoo and R. Balasubramaniam, "Mechanical behavior of novel phosphoric irons for concrete reinforcement applications," *Scr. Mater.*, vol. 56, no. 2, pp. 117–120, 2007.
[11] H. Erhart and H. J. Grabke, "Site competition in grain boundary segregation of phosphorus and nitrogen in iron," *Scr. Metall.*, vol. 15, no. 5, pp. 531–534, 1981.
[12] G. Sahoo, B. Singh, and A. Saxena, "Characterization of high phosphorous containing hot rolled weather resistant structural steels," *Mater. Sci. Eng. A*, vol. 628, no. January, pp. 303–310, 2015.
[13] H. Liu, C. M. Abiko, K. Kimura, "Effect of silicon on the grain boundary segregation of phosphorus and the phosphorus induced intergranular fracture in high purity Fe-Si-P Alloys," in *Strength of metals and alloys (ICSMA 8), volume 3, Proceedings of the 8th international conference on the strength of metals and alloys, Tampere, Finland, 22-26 Aug. 1988,* 1989, pp. 1101–1106.
[14] G. Sahoo and R. Balasubramaniam, "On the corrosion behaviour of phosphoric irons in simulated concrete pore solution," *Corros. Sci.*, vol. 50, no. 1, pp. 131–143, 2008.
[15] R. P. L. Bertolini, B. Elsener, P. Pedeferri, *Corrosion of Steel in Concrete*. Weinheim, Germany: Wiley-VCH Verlag GmbH & Co., 2004.
[16] B. B. Hope and A. K. C. Ip, "Chloride corrosion threshold in concrete," *ACI Mater. J.*, vol. 84, no. 4, pp. 306–314, 1987.
[17] M. E. Saremi, M., "A study on chloride-induced depassivation of mild steel in simulated concrete pore solution," *Cem. Concr. Res.*, vol. 32, no. 12, pp. 1915–1921, 2002.
[18] K. K. Sagoe-Crentsil, F. P. Glasser, and J. T. S. Irvine, "Electrochemical characteristics of reinforced concrete as determined by impedance spectroscopy," *Br. Corros. J.*, vol. 27, no. 2, pp. 113–118, 1992.
[19] M. I. Jafar, J. L. Dawson, and D. G. John, "Electrochemical impedance and harmonic analysis

measurements on steel in concrete; Electrochemical Impedance: Analysis and Interpretation, ASTM STP 1188; ed. John R Scully, David Silverman, Martin W Kendig," Philadelphia, PA, 1993.

[20] D. Trejo and P. J. Monteiro, "Corrosion performance of conventional (ASTM A615) and low-alloy (ASTM A706) reinforcing bars embedded in concrete and exposed to chloride environments," *Cem. Concr. Res.*, vol. 35, no. 3, pp. 562–571, 2005.

[21] T. P. Hoar, "The production and breakdown of the passivity of metals," *Corros. Sci.*, vol. 7, no. 6, pp. 341–355, 1967.

[22] C. Q. Ye, R. G. Hu, S. G. Dong, X. J. Zhang, R. Q. Hou, R. G. Du, C. J. Lin, and J. S. Pan, "EIS analysis on chloride-induced corrosion behavior of reinforcement steel in simulated carbonated concrete pore solutions," *J. Electroanal. Chem.*, vol. 688, pp. 275–281, 2013.

[23] M. Janik-Czachor, A. Szummer, and Z. Szklarska-Smialowska, "Electron microprobe investigation of processes leading to the nucleation of pits on iron," *Corros. Sci.*, vol. 15, no. 12, pp. 775–778, 1975.

[24] J. A. Gomez, Mejia, J. Antonissen, C. A. Palacio, and E. De Grave, "Effects of Si as alloying element on corrosion resistance of weathering steel," *Corros. Sci.*, vol. 59, pp. 198–203, 2012.

[25] H. J. Grabke, "The Role of Nitrogen in the Corrosion of Iron and Steels.," *ISIJ Int.*, vol. 36, no. 7, pp. 777–786, 1996.

[26] J. Flis, I. Flis-Kabulska, and T. Zakroczymski, "Corrosion and passivation of iron and its nitrided layer in borate buffer," *Electrochim. Acta*, vol. 54, no. 6, pp. 1810–1819, 2009.

[27] P. Gu, S. Elliott, R. Hristova, J. J. Beaudoin, R. J. Brousseau, and B. Baldock, "A Study of corrosion inhibitor performance in chloride contaminated concrete by electrochemical impedance spectroscopy," *ACI Mater. J.*, vol. 94, no. 5, pp. 385–395, 1997.

[28] J. M. R. Génin, L. Dhouibi, P. Refait, M. Abdelmoula, and E. Triki, "Influence of phosphate on corrosion products of iron in chloride-polluted-concrete-simulating solutions: Ferrihydrite vs green rust," *Corrosion*, vol. 58, no. 6, pp. 467–478, 2002.

[29] D. A. Jone, *Principles and Prevention of Corrosion*. New York: Macmillan Publishing Company, 1992.

[30] C. Alonso, C. Andrade, M. Castellote, and P. Castro, "Chloride threshold values to depassivate reinforcing bars embedded in a standardized OPC mortar," *Cem. Concr. Res.*, vol. 30, no. 7, pp. 1047–1055, 2000.

[31] M. Moreno, W. Morris, M. G. Alvarez, and G. S. Duffo, "Corrosion of reinforcing steel in simulated concrete pore solutions effect of carbonation and chloride content," *Corros. Sci.*, vol. 46, no. 11, pp. 2681–2699, 2004.

[32] B. MacDougall and M. J. Graham, *Growth and stability of passive films, in: Corrosion Mechanism in Theory and Practice*. New York: Marcel Dekker, 1995.

[33] R. G. Kelly, J. R. Scully, D. W. Shoesmith, and R. G. Buchheit, *Electrochemical Techniques in Corrosion Science and Engineering*. New York: Marcel Dekker, 2003.

[34] M. Keddam, M. Krarti, and C. Pallotta, "Some Aspects of the Fluctuations of the Passive Current on Stainless Steel in Presence of Chlorides - Their Relation To the Probalistic Approach of Pitting Corrosion.," *Corrosion*, vol. 43, no. 8, pp. 454–458, 1987.

[35] G. W. Walter, "A review of impedance plot methods used for corrosion performance analysis of painted metals," *Corros. Sci.*, vol. 26, no. 9, pp. 681–703, 1986.

[36] F. Mansfeld, V. Wang, and H. Shih, "Development of stainless Aluminum," *J. Electrochem. Soc.*, vol. 138, no. 12, pp. L74–L75, 1991.

[37] O. Poupard, A. Ait-Mokhtar, and P. Dumargue, "Corrosion by chlorides in reinforced concrete: Determination of chloride concentration threshold by impedance spectroscopy," *Cem. Concr. Res.*, vol. 34, no. 6, pp. 991–1000, 2004.

[38] B. Cox and Y.-M. Wong, "Simulating porous oxide films on zirconium alloys," *J. Nucl. Mater.*, vol. 218, no. 3, pp. 324–334, 1995.

[39] M. Cai and S. Park, "Oxidation of Zinc in alkaline solutions studied by Electrochemical

Impedance Spectroscopy," *J. Electrochem. Soc.*, vol. 143, no. 12, pp. 3895–3902, 1996.
[40] J. A. Bardwell and M. C. H. McKubre, "ac Impedance spectroscopy of the anodic film on zirconium in neutral solution," *Electrochim. Acta*, vol. 36, no. 3–4, pp. 647–653, 1991.
[41] J. Zhang, J. Hu, J. Zhang, and C. Cao, "Studies of water transport behavior and impedance models of epoxy-coated metals in NaCl solution by EIS," *Prog. Org. Coatings*, vol. 51, no. 2, pp. 145–151, 2004.
[42] W. Chen, R. Du, C. Ye, Y. Zhu, and C. Lin, "Study on the corrosion behavior of reinforcing steel in simulated concrete pore solutions using in situ Raman spectroscopy assisted by electrochemical techniques," *Electrochim. Acta*, vol. 55, no. 20, pp. 5677–5682, 2010.
[43] J. Cruz, T. Pandiyan, and E. Garcı, "A new inhibitor for mild carbon steel : Electrochemical and DFT studies," *J. Electroanal. Chem.*, vol. 583, no. 1, pp. 8–16, 2005.
[44] X. Feng, Y. Tang, and Y. Zuo, "Influence of stress on passive behaviour of steel bars in concrete pore solution," *Corros. Sci.*, vol. 53, no. 4, pp. 1304–1311, 2011.
[45] C. M. Abreu, M. J. Cristóbal, R. Losada, X. R. Nóvoa, G. Pena, and M. C. Pérez, "Comparative study of passive films of different stainless steels developed on alkaline medium," *Electrochim. Acta*, vol. 49, no. 17–18, pp. 3049–3056, 2004.
[46] L. Hamadou, A. Kadri, and N. Benbrahim, "Characterisation of passive films formed on low carbon steel in borate buffer solution (pH 9.2) by electrochemical impedance spectroscopy," *Appl. Surf. Sci.*, vol. 252, no. 5, pp. 1510–1519, 2005.
[47] D. E. Williams, T. F. Mohiuddin, and Y. Y. Zhu, "Elucidation of a trigger mechanism for pitting corrosion of stainless steels using submicron resolution scanning electrochemical and photoelectrochemical microscopy," *J. Electrochem. Soc.*, vol. 145, no. 8, pp. 2664–2672, 1998.
[48] J. Van Muylder and M. Pourbaix, *Establishment and interpretation of potential-pH equilibrium diagram of Fe, first ed., Atlas of electrochemical equilibria in aqueous solutions,*. Cebelcor Brussels: Pergamon Press, 1966.
[49] G. H. Awad and T. P. Hoar, "The role of phosphates in inhibiting pitting of commercial mild steel in chloride-containing media," *Corros. Sci.*, vol. 15, no. January 1974, pp. 581–588, 1975.
[50] T. Misawa, "The thermodynamic consideration for Fe-H2O system at 25 ° C," *Corros. Sci.*, vol. 13, no. November 1972, pp. 659–676, 1973.
[51] S. Virtanen, B. Elsener, and H. Bohni, "Effect of metalloids Fe-Cr alloys," *J. less common Met.*, vol. 145, pp. 581–593, 1988.
[52] R. Nishimura, M. Araki, and K. Kudo, "Breakdown of Passive Film on lron," *Corrosion*, vol. 40, no. 9, pp. 465–470, 1984.